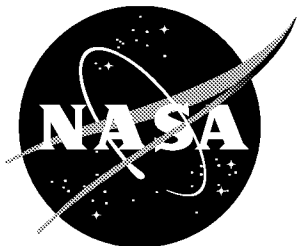


NASA/TM-1999-209116



A Novel Shape Parameterization Approach

Jamshid A. Samareh
Langley Research Center, Hampton, Virginia

May 1999

The NASA STI Program Office ...in Profile

Since its founding, NASA has been dedicated to the advancement of aeronautics and space science. The NASA Scientific and Technical Information (STI) Program Office plays a key part in helping NASA maintain this important role.

The NASA STI Program Office is operated by Langley Research Center, the lead center for NASA's scientific and technical information. The NASA STI Program Office provides access to the NASA STI Database, the largest collection of aeronautical and space science STI in the world. The Program Office is also NASA's institutional mechanism for disseminating the results of its research and development activities. These results are published by NASA in the NASA STI Report Series, which includes the following report types:

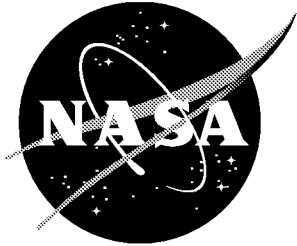
- **TECHNICAL PUBLICATION.** Reports of completed research or a major significant phase of research that present the results of NASA programs and include extensive data or theoretical analysis. Includes compilations of significant scientific and technical data and information deemed to be of continuing reference value. NASA counterpart and peer-reviewed formal professional papers, but having less stringent limitations on manuscript length and extent of graphic presentations.
- **TECHNICAL MEMORANDUM.** Scientific and technical findings that are preliminary or of specialized interest, e.g., quick release reports, working papers, and bibliographies that contain minimal annotation. Does not contain extensive analysis.
- **CONTRACTOR REPORT.** Scientific and technical findings by NASA-sponsored contractors and grantees.
- **CONFERENCE PUBLICATION.** Collected papers from scientific and technical conferences, symposia, seminars, or other meetings sponsored or co-sponsored by NASA.
- **SPECIAL PUBLICATION.** Scientific, technical, or historical information from NASA programs, projects, and missions, often concerned with subjects having substantial public interest.
- **TECHNICAL TRANSLATION.** English-language translations of foreign scientific and technical material pertinent to NASA's mission.

Specialized services that complement the STI Program Office's diverse offerings include creating custom thesauri, building customized databases, organizing and publishing research results...even providing videos.

For more information about the NASA STI Program Office, see the following:

- Access the NASA STI Program Home Page at **<http://www.sti.nasa.gov>**
- E-mail your question via the Internet to help@sti.nasa.gov
- Fax your question to the NASA STI Help Desk at (301) 621-0134
- Phone the NASA STI Help Desk at (301) 621-0390
- Write to:
NASA STI Help Desk
NASA Center for Aerospace Information
7121 Standard Drive
Hanover, MD 21076-1320

NASA/TM-1999-209116



A Novel Shape Parameterization Approach

Jamshid A. Samareh
Langley Research Center, Hampton, Virginia

National Aeronautics and
Space Administration

Langley Research Center
Hampton, Virginia 23681-2199

May 1999

Available from:

NASA Center for AeroSpace Information (CASI)
7121 Standard Drive
Hanover, MD 21076-1320
(301) 621-0390

National Technical Information Service (NTIS)
5285 Port Royal Road
Springfield, VA 22161-2171
(703) 605-6000

A Novel Shape Parameterization Approach

Jamshid A. Samareh*

NASA Langley Research Center, Hampton, VA 23681

This paper presents a novel parameterization approach for complex shapes suitable for a multidisciplinary design optimization application. The approach consists of two basic concepts: (1) parameterizing the shape perturbations rather than the geometry itself and (2) performing the shape deformation by means of the soft objects animation algorithms used in computer graphics. Because the formulation presented in this paper is independent of grid topology, we can treat computational fluid dynamics and finite element grids in a similar manner. The proposed approach is simple, compact, and efficient. Also, the analytical sensitivity derivatives are easily computed for use in a gradient-based optimization. This algorithm is suitable for low-fidelity (e.g., linear aerodynamics and equivalent laminated plate structures) and high-fidelity analysis tools (e.g., nonlinear computational fluid dynamics and detailed finite element modeling). This paper contains the implementation details of parameterizing for planform, twist, dihedral, thickness, and camber. The results are presented for a multidisciplinary design optimization application consisting of nonlinear computational fluid dynamics, detailed computational structural mechanics, performance, and a simple propulsion module.

Nomenclature

| | |
|--------------------|---|
| A | wing area |
| AR | wing aspect ratio |
| B | Bernstein polynomial |
| b | wing span |
| C | chord |
| c | camber |
| d | degree |
| e | scale factor for twist and shearing |
| N | B-spline basis function |
| \bar{n} | normal vector |
| \bar{P} | coordinates of NURBS control point |
| \bar{R} | coordinates of deformed model |
| \bar{r} | coordinates of baseline model |
| \bar{S} | shearing vector |
| \bar{T} | twist plane |
| t | thickness |
| u | parameter coordinate |
| \bar{v} | design variable vector |
| W | NURBS weights |
| X, Y, Z | Cartesian coordinates of deformed model |
| x, y, z | Cartesian coordinates of baseline model |
| α | angle of attack, deg |
| Δ | total deformation |
| δ | deformation |
| θ | twist angle, deg |
| Λ | leading edge sweep angle, deg |
| λ | wing taper ratio |
| ξ, η, ζ | coordinates of deformation object |
| ρ | twist radius |

Subscripts

| | |
|----|--------|
| ca | camber |
|----|--------|

| | |
|-----------|---|
| I, J, K | total numbers of control points |
| i, j, k | indices for NURBS control point |
| L | wing lower surface |
| le | leading edge |
| m | center |
| p | degree of B-spline basis function in i direction |
| pl | planform |
| q | degree of B-spline basis function in ij direction |
| r | root |
| sh | shear |
| te | trailing edge |
| t | tip |
| th | thickness |
| tw | twist |
| U | wing upper surface |

Superscripts

| | |
|-----|-------------------------|
| T | transpose of the matrix |
|-----|-------------------------|

Introduction

MULTIDISCIPLINARY design optimization (MDO) methodology seeks to exploit the synergism of mutually interacting phenomena to create improved designs. An MDO process commonly involves sizing, topology and shape design variables. Multidisciplinary shape optimization (MSO) finds the optimum shape for a given structural layout. It is a challenging task to perform MSO for a complete airplane configuration with high-fidelity analysis tools. The analysis models, also referred to as grids or meshes, are based on some or all of the airplane components, such as skin, ribs, and spars. The aerodynamic analysis uses the detailed definition of the skin, also referred to as the outer mold line (OML), whereas the computational structural mechanics (CSM) models use all components. Generally, the structural model requires a relatively coarse grid, but

*Research Scientist, Multidisciplinary Optimization Branch, Mail Stop 159, j.a.samareh@larc.nasa.gov.

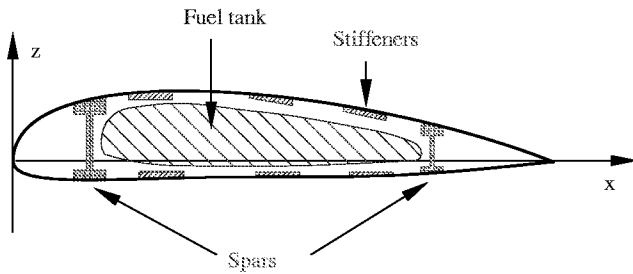


Fig. 1 Internal components of a wing.

it must handle very complex internal and external geometries. In contrast, the computational fluid dynamics (CFD) grid is a very fine one, but it only needs to model the external geometry. The MSO of an airplane must treat not only the wing skin, fuselage, flaps, nacelles, and pylons, but also the internal structural elements such as spars and ribs (see Fig. 1). The treatment of internal structural elements is especially important for detailed finite element (FE) analysis. For a high-fidelity MSO process to be successful, the process must be based on a compact and effective set of design variables that yields a feasible configuration. For more details, readers are referred to an overview paper by this author¹ on geometry modeling and grid generation for design and optimization.

The model parameterization is the first step for an MSO process. Over the past several decades, shape optimization has been successfully applied for two-dimensional and simple three-dimensional configurations. The recent advances in computer hardware and software have made MSO applications more feasible for complex configurations. An important ingredient of aerodynamic shape optimization is the availability of a model parameterized with respect to the aerodynamic parameters such as planform, twist, shear, camber, and thickness. The parameterization techniques can be divided into the following categories:² discrete, polynomial and spline, computer-aided design (CAD), analytical, and deformation. Readers are referred to reports by Haftka,³ Ding,⁴ and Samareh² for surveys of shape optimization and parameterization.

In a multidisciplinary application, the parameterization must be compatible and adaptable to various analysis tools ranging from low-fidelity tools, such as linear aerodynamics and equivalent laminated plate structures, to high-fidelity tools, such as nonlinear CFD and detailed CSM codes. Creation of CFD and CSM grids is time-consuming and costly for a full airplane model: it takes several months to develop detailed CSM and CFD grids based on a CAD model. To fit the MSO process into the product development cycle times, the MSO must rely on the parameterization of the analysis grids. For a multidisciplinary problem, the process must also use a geometry model and parameterization consistently across all disciplines. For use with

gradient-based optimization, the geometry model must provide accurate sensitivity derivatives of the analysis model with respect to design variables.

This paper presents an approach for shape parameterization suitable for a multidisciplinary design optimization application. The approach consists of two basic concepts. The first concept is based on parameterizing the shape perturbation rather than the geometry itself. The second concept is based on using the soft object animation⁵ (SOA) algorithms for shape parameterization. The combined algorithm, initially introduced by this author,⁶ was successfully implemented for aerodynamic shape optimization with analytical sensitivity with structured grid^{7,8} and unstructured⁹ grid CFD codes.

Parameterizing the Shape Perturbations

At first sight parameterization by splines may seem to be a viable approach for shape parameterization. The spline representation uses a set of control points to define any shape. These control points could be used as design variables for optimization. Typically over a hundred control points are required to define an airfoil section and over 20 airfoil sections to define a conventional wing. This requirement results in over two thousand control points (i.e., six thousand shape design variables) for a simple wing. The number of control points is even larger for a complete airplane model created with a commercial CAD system. The large number of control points is needed more for the accuracy than for the complexity.

Even if we could afford to use a large number of design variables, the automatic regeneration of analysis models (e.g., CSM and CFD grids) is not possible with the current technology. For example, it takes several months to create an accurate CSM model of an airplane. Also, traditional shape parameterization processes parameterize only the OML and are ineffective in parameterizing internal components such as spars, ribs, stiffeners, and fuel tanks (see Fig. 1).

It is possible to use any shape (e.g., a sphere) as the initial wing definition, allowing the optimizer to find the optimum wing shape; however, it is not a common practice. Typically, the optimization starts with an existing wing design, and the goal is to improve the wing performance by using numerical optimization. The geometry changes (perturbations) between initial and optimized wing are very small,^{10,11} but the difference in wing performance can be substantial. An effective way to reduce the number of shape design variables is to parameterize the shape perturbations instead of parameterizing the shape itself. Throughout the optimization cycles, the analysis grid can be updated as

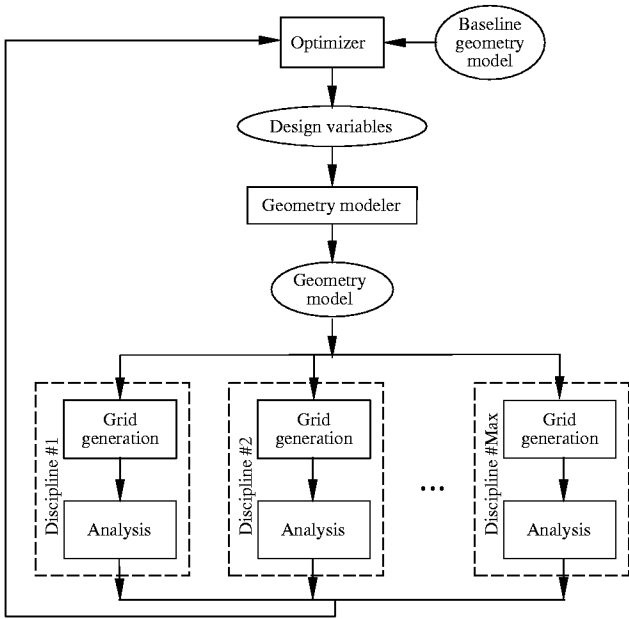


Fig. 2 A typical MSO process.

$$\bar{R}(\bar{v}) = \bar{r} + \Delta\bar{R}(\bar{v}) \quad (1)$$

where \bar{r} is the baseline grid, \bar{R} is the deformed (perturbed) grid, $\Delta\bar{R}$ is the change (perturbation), and \bar{v} is the design variable vector. The change, $\Delta\bar{R}$, is a combination of changes in thickness, camber, twist, shear, and planform:

$$\Delta\bar{R} = \delta\bar{R}_{th} + \delta\bar{R}_{ca} + \delta\bar{R}_{tw} + \delta\bar{R}_{sh} + \delta\bar{R}_{pl} \quad (2)$$

It takes far fewer design variables to parameterize the shape perturbation $\Delta\bar{R}$ than \bar{r} itself.

Figures 2-3 contrast the typical and modified MSO processes. In a typical MSO process (Fig. 2), a geometry modeler perturbs the baseline geometry model. Because automatic grid generation tools are not available for all disciplines, it would be very difficult to automate this MSO process. In contrast, the modified MSO process (Fig. 3) relies on parameterizing the baseline grids, hence making it possible to automate the entire MSO process.

Soft Object Animation

The field of SOA in computer graphics⁵ provides algorithms for morphing images¹² and deforming models.^{13,14} These algorithms are powerful tools for modifying shapes: they use a high-level shape deformation, as opposed to manipulation of lower level geometric entities. Hall¹² presented an algorithm and provided computer codes for morphing images. The deformation algorithms are suitable for deforming models represented by either a set of polygons or a set of parametric curves and surfaces. The SOA algorithms treat the model as rubber that can be twisted, bent, tapered,

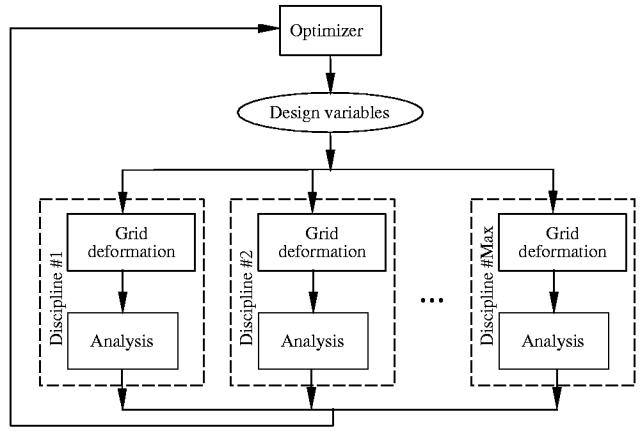


Fig. 3 The modified MSO process.

compressed, or expanded, while retaining its topology. This is ideal for parameterizing airplane models that have external skin as well as internal components (e.g., see Fig. 1). The SOA algorithms relate vertices of an analysis model (grid) to a small number of design variables. Consequently, the SOA algorithms can serve as the basis for an efficient shape parameterization technique.

Barr¹³ presented a deformation approach in the context of physically based modeling. This approach uses physical simulation to obtain realistic shape and motions and is based on operations such as translation, rotation, and scaling. With this algorithm, the deformation is achieved by moving the vertices of a polygon model or the control points of a parametric curve and surface. Sederberg and Parry¹⁴ presented another approach for deformation based on the free-form deformation (FFD) algorithm that operates on the whole space regardless of the representation of the deformed objects embedded in the space. The algorithm allows a user to manipulate the control points of trivariate B-spline volumes. The disadvantage of FFD is that the design variables may have no physical significance for the design engineers. This drawback makes it difficult to select an effective and compact set of design variables. This report presents a set of modifications to the original SOA algorithms to alleviate this and other drawbacks.

For the modified SOA algorithms presented in the next several sections, implementation will include the following common set of steps:

1. Select an appropriate deformation technique and object. This defines the forward mapping from the deformation object coordinate system (ξ, η, ζ) to the baseline grid coordinate system (x, y, z) .
2. Establish a backward mapping from the baseline grid coordinate system (x, y, z) to the deformation object coordinate system (ξ, η, ζ) . The ξ, η, ζ mapping parameters are fixed and are independent of the shape perturbations. This is a preprocessing step that is required only once.

3. Perturb the control parameters (design variables) defining the deformation object.
4. Evaluate the grid perturbation ($\Delta\bar{R}$) using the ξ, η, ζ parameters.

The following sections provide recipes for using SOA algorithms for parameterizing airplane models for thickness, camber, twist, shear, and planform changes.

Thickness and Camber

We use a nonuniform rational B-spline (NURBS) representation as the deformation object for thickness and camber parameterization. The NURBS representation combines the desirable properties of National Advisory Committee for Aeronautics (NACA) definition¹⁵ and spline techniques, and it does not deteriorate or destroy the smoothness of the initial geometry. Readers should consult the textbook by Farin¹⁶ for a detailed discussion on NURBS.

The changes in thickness and camber are represented by

$$\delta\bar{R}_{th}(\xi, \eta) = \frac{\sum_{i=0}^I N_{i,p}(\xi) \sum_{j=0}^J N_{j,q}(\eta) W_{i,j} \bar{P}_{th,i,j}}{\sum_{i=0}^I N_{i,p}(\xi) \sum_{j=0}^J N_{j,q}(\eta) W_{i,j}} \quad (3)$$

$$\delta\bar{R}_{ca}(\xi, \eta) = \frac{\sum_{i=0}^I N_{i,p}(\xi) \sum_{j=0}^J N_{j,q}(\eta) W_{i,j} \bar{P}_{ca,i,j}}{\sum_{i=0}^I N_{i,p}(\xi) \sum_{j=0}^J N_{j,q}(\eta) W_{i,j}} \quad (4)$$

where $\bar{P}_{th,i,j}$ and $\bar{P}_{ca,i,j}$ are control points (forming a control surface) for thickness and camber, $W_{i,j}$ are the weights, and $N_{i,p}$ and $N_{j,q}$ are the p and q degree B-spline basis functions defined on the nonperiodic and nonuniform knot vectors. Figures 4-5 show the NURBS control points in (ξ, η) and (x, y, z) coordinate systems, respectively. The control points and weights could be used as design variables.

The NURBS representation has several important properties for design and optimization. A NURBS curve of order p , having no multiple interior knots, is $p - 2$ differentiable. As a result, the NURBS representation can handle a complex deformation and still maintain smooth surface curvature. Readers are referred to the textbook by Farin¹⁶ for details on the properties of NURBS representation. The control points are the coefficients of the basis functions, but the smoothness is controlled by the basis functions, not the control points. The NURBS representation is local in nature, allowing the surface to be deformed locally, hence leaving the rest of the surface unchanged. Equations 3 and 4 serve as the forward mapping between the thickness and camber design variables and the grid perturbation ($\delta\bar{R}_{th}, \delta\bar{R}_{ca}$).

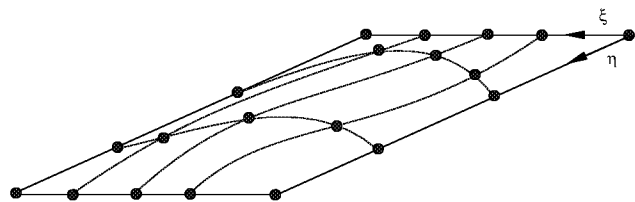


Fig. 4 Thickness and camber definitions in wing coordinate system.

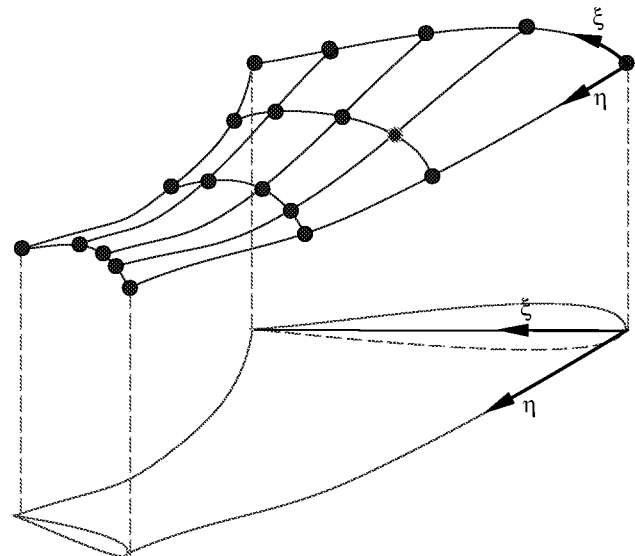


Fig. 5 Thickness and camber definitions in $x, y,$ and z coordinate system.

The next step is to establish the backward mapping from the deformation object (i.e., NURBS surface) coordinates (ξ, η) to the baseline model coordinates (x, y, z) . The wing coordinate system—percent chord and span—is a good candidate. The percentage chord, $\%c$, is used for ξ , and the spanwise location, y , is used for η .

$$\xi = \%c, \quad \eta = y \quad (5)$$

To calculate $\%c$, we need to determine the wing chord at each y station. The baseline CAD model provides the leading edge ($\bar{R}_{le}(\eta)$), trailing edge ($\bar{R}_{te}(\eta)$), wing center $\bar{R}_m(\eta)$, and normal vector defining the airfoil plane $\bar{T}(\eta)$ as shown in Fig. 6. The curve defining the wing center does not have to be at the center of the wing, but it should be somewhere between the upper and the lower wing surfaces. The $\bar{R}_{le}(\eta)$, $\bar{R}_{te}(\eta)$, and $\bar{R}_m(\eta)$ are used to separate points on the upper surface from points on the lower surface.

Because we know η for each grid point, we can define a plane that passes through the grid point with a normal vector defined by $\bar{T}(\eta)$. We must find the intersection of this plane and the curves shown in Fig. 6,

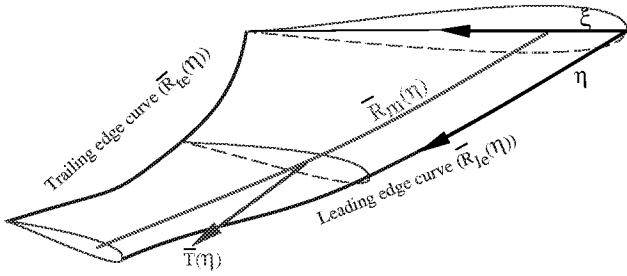


Fig. 6 Curves defining the backward mapping.

$$\bar{T}(\eta) \cdot [\bar{r} - \bar{R}_{te}(\eta)]^T = 0 \quad (6)$$

$$\bar{T}(\eta) \cdot [\bar{r} - \bar{R}_{le}(\eta)]^T = 0 \quad (7)$$

$$\bar{T}(\eta) \cdot [\bar{r} - \bar{R}_m(\eta)]^T = 0 \quad (8)$$

Equations 6-8 must be solved for all grid points in the model. For a high-order NURBS curve, Eqs. 6-8 are nonlinear and can be solved by the Newton-Raphson method. The solution to Eqs. 6-8 for each η is a set of three points located at the leading edge, the trailing edge, and the center. The %c is calculated based on the leading and trailing edge points. Next, we need to separate the grid points defining the wing model into upper and lower. We can connect the three points obtained from Eqs. 6-8 to form a curve that separates the upper surface from the lower surface. This curve does not have to represent the camber line accurately, and a wing with drooping leading edge or with highly cambered airfoil sections may require more than one $\bar{R}_m(\eta)$ to define the curve. With this approach, it is possible to localize the deformation to a specific design area by setting allowable %c_{min}, %c_{max}, η_{min} , and η_{max} .

As the design variables (control points $\bar{P}_{i,j}$) change, we can calculate the contribution from the thickness and camber by Eqs. 3-4. The advantage of this process is that the sensitivity of grid point location with respect to design variables is only a function of the B-spline basis functions,

$$\frac{\partial \bar{R}}{\partial \bar{P}_{th, id, jd}} = \frac{\partial \bar{R}}{\partial \bar{P}_{ca, id, jd}} = \frac{N_{id,p}(\xi) N_{jd,q}(\eta) W_{id,jd}}{\sum_{i=0}^I N_{i,p}(\xi) \sum_{j=0}^J N_{j,q}(\eta) W_{i,j}} \quad (9)$$

where id and jd are the indices of design variables, $\bar{P}_{id,jd}$. Consequently the sensitivity, as seen in Eq. 9, is independent of the design variables ($\bar{P}_{id,jd}$) and the coordinates (x, y, z) . Thus, we need to calculate the sensitivity with respect to thickness and camber only at the beginning of the optimization.

Twist and Shear

The twist angle is defined as the difference between the airfoil section incident angle at the root and each

airfoil section incident angle. Similarly, the shear (dihedral) is defined as the difference between the airfoil leading edge z coordinate for the root and the z coordinate at each airfoil section. If the twist angle at the tip is less than the twist at the root, the wing is said to have a washout, which could delay the stall at the wing tip. Also, as the wing washout increases, the wing load shifts from outboard to inboard. As a result, the spanwise distribution of the twist angle plays an important role in the wing performance.

The SOA are used to modify the wing twist and shear distribution. Alan Barr presented a series of SOA algorithms for twisting, bending, and tapering an object.¹³ Watt and Watt referred to these algorithms as nonlinear global deformation.⁵ Sederberg and Greenwood extended Barr's ideas to handle complex shapes.¹⁷ Modified versions of these algorithms are presented in this paper.

To modify the twist and shear distributions, the wing is embedded in a nonlinear deformation object referred to as a twist cylinder, that is shown in Fig. 7. The twist cylinder is also used for modifying shear distribution. The center of the cylinder is defined by a NURBS curve, $\bar{R}_m(\eta)$. The effect of deformation can be confined to a section of a wing by limiting the parameter η to vary between η_{min} and η_{max} . The η_{min} can extend to the wing root, and the η_{max} can go beyond the wing tip. The cylinder can be twisted and sheared only in a plane (twist plane) defined by a point along $\bar{R}_m(\eta)$ with a normal vector of $\bar{T}(\eta)$. The $\rho_i(\eta)$ and $\rho_o(\eta)$ are the radii of inner and outer cylinders, respectively (see Fig. 7). The deformation has no effect for grid points located outside of the outer cylinder, and the effect of deformation is scaled linearly from the outer cylinder to the inner cylinder. This allows us to blend the deformed region with the undeformed region in a continuous manner.

The angle $\theta(\eta)$ defines the desired twist angle distribution, and $\bar{S}(\eta)$ defines the shearing vector. The $\theta(\eta)$ and $\bar{S}(\eta)$ variables are defined by NURBS representation:

$$\theta(\eta) = \frac{\sum_{i=0}^I N_{i,p}(\eta) W_i \theta_i}{\sum_{i=0}^I N_{i,p}(\eta) W_i} \quad (10)$$

$$\bar{S}(\eta) = \frac{\sum_{i=0}^I N_{i,p}(\eta) W_i \bar{S}_i}{\sum_{i=0}^I N_{i,p}(\eta) W_i} \quad (11)$$

where θ_i and \bar{S}_i are the twist and shear design variables, respectively. Similar to thickness and camber algorithms, we use

$$\eta = y, \quad \bar{T}(\eta) = (0, y, 0)^T \quad (12)$$

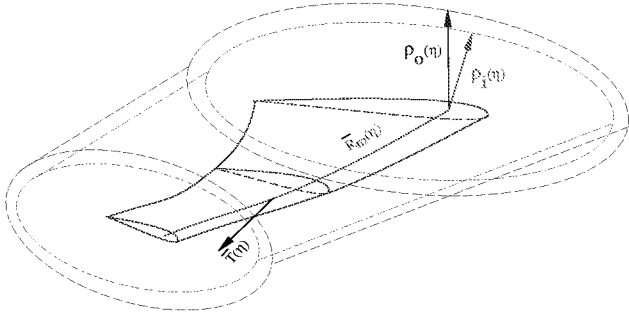


Fig. 7 Twist definition.

The second step for twist and shear deformation is to establish the forward mapping from the deformation object (twist cylinder) coordinate system (η) to the model coordinate system (x, y, z). We use Eq. 8 to determine η . Once η is determined, we can calculate the local $\rho(\eta)$, $\rho_i(\eta)$, $\rho_o(\eta)$, $\bar{T}(\eta)$, $\theta(\eta)$, and $\bar{S}(\eta)$. The point \bar{r} is rotated $\theta(\eta)$ degrees about $\bar{R}_m(\eta)$ and sheared \bar{S} .

$$\delta \bar{R}_{tw}(\eta) = e(\eta) \rho(\eta) [\sin \theta(\eta), 0, \cos \theta(\eta)]^T \quad (13)$$

$$\delta \bar{R}_{sh}(\eta) = e(\eta) \bar{S}(\eta) \quad (14)$$

where $e(\eta)$ is a scale factor which diminishes the effect of deformation as we approach the outer cylinder.

$$e(\eta) = \begin{cases} 0 & \text{if } \rho(\eta) \geq \rho_o(\eta) \\ \frac{\rho(\eta) - \rho_o}{\rho_i(\eta) - \rho_o} & \text{if } \rho_i \leq \rho(\eta) < \rho_o(\eta) \\ 1 & \text{if } \rho(\eta) < \rho_i \end{cases} \quad (15)$$

The sensitivity of a grid point with respect to the twist and shear design variables is

$$\frac{\partial \bar{R}}{\partial \theta_i} = e(\eta) \rho(\eta) \frac{\partial \theta(\eta)}{\partial \theta_i} [\cos \theta(\eta), 0, -\sin \theta(\eta)]^T \quad (16)$$

$$\frac{\partial \bar{R}}{\partial \bar{S}_i} = e(\eta) \frac{\partial \bar{S}(\eta)}{\partial \bar{S}_i} \quad (17)$$

The term $\frac{\partial \theta(\eta)}{\partial \theta_i}$ is independent of the twist design variables θ_i (see Eq. 10). However, $\sin \theta(\eta)$ and $\cos \theta(\eta)$ depend on the twist design variables and must be updated every cycle of the optimization. In contrast, the term $\frac{\partial \bar{S}(\eta)}{\partial \bar{S}_i}$ is independent of shear design variables \bar{S}_i (see Eq. 11).

Figure 8 shows the inner twist cylinder for a commercial transport. Figure 9 shows the result of twisting the wing 45° at the tip. This is a large and unrealistic amount of twist, but it shows the effectiveness of the SOA.

Planform Parameterization

The wing planform is typically modeled with a set of two-dimensional trapezoids in the x-y plane. Figure 10

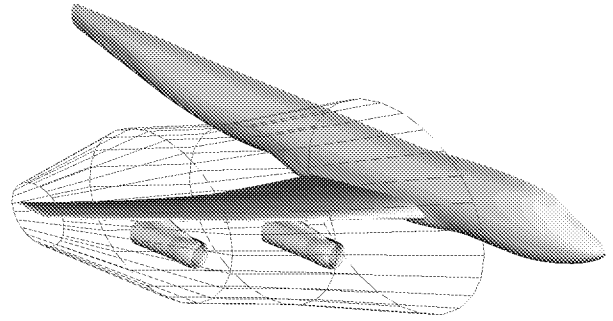


Fig. 8 Twist definition for a transport.

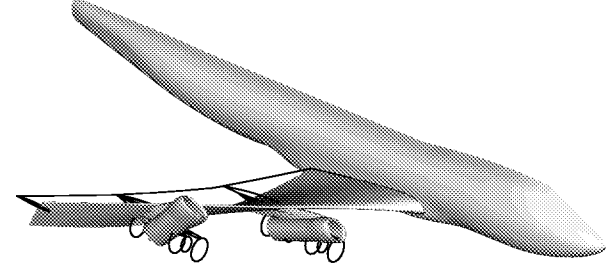


Fig. 9 Result of 45° twist on a transport.

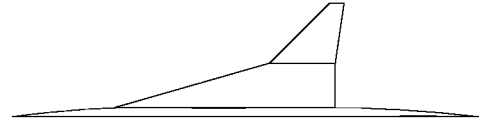


Fig. 10 Planform of a generic high-speed civil transport.

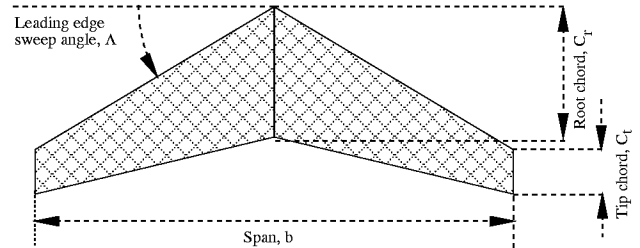


Fig. 11 Planform definition.

shows the planform of a generic high-speed civil transport that uses two trapezoids. As shown in Fig. 11, each trapezoid is defined by the root chord (C_r), tip chord (C_t), span (b), and sweep angle (Λ). From these, other planform parameters, such as area (A), aspect ratio (AR), and taper ratio (λ), are defined:

$$A = \frac{b}{2}(C_r + C_t), \quad AR = \frac{b^2}{A}, \quad \lambda = \frac{C_t}{C_r} \quad (18)$$

The FFD algorithm described by Sederberg and Parry¹⁴ is ideal for deforming the polygonal models. Like other SOA algorithms, this algorithm maintains the polygon connectivity, and the deformation is applied only to the vertices of the model. The FFD

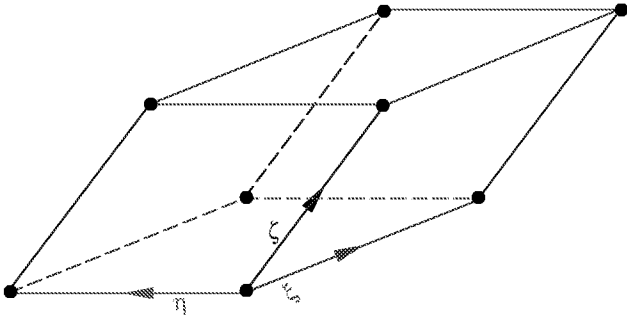


Fig. 12 Parallelepiped volume for free-form deformation.

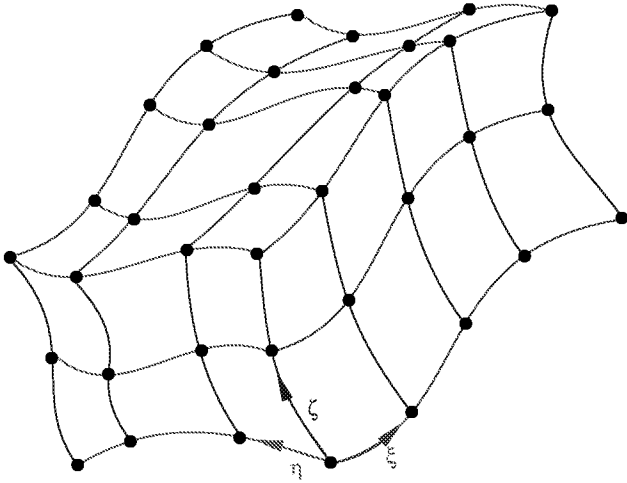


Fig. 13 NURBS volume for free-form deformation.

process is similar to embedding the grid inside a block of clear, flexible plastic (deformation object) so that, as the plastic is deformed, the grid is deformed as well. Deformation of complex shapes may require several deformation objects. The shape of these deformation objects is not arbitrary. In fact, they must be three-dimensional parametric volumes, which could range from a parallelepiped as shown in Fig. 12 to a general NURBS volume as shown in Fig. 13. The block is deformed by perturbing the vertices that control the shape of the deformation block (e.g., corners of the parallelepiped). For parametric volume blocks, parameters controlling the deformation are related through the mapping coordinates (ξ, η, ζ) . These coordinates are used in both forward and backward mapping.

Figure 12 shows a general parallelepiped defined by a set of control points forming three primary edges or directions along ξ , η , and ζ . The relation for a parallelepiped is defined as

$$\bar{r}(\xi, \eta, \zeta) = \bar{P}_0 + \bar{n}_\xi \xi + \bar{n}_\eta \eta + \bar{n}_\zeta \zeta \quad (19)$$

where \bar{P}_0 is the origin of the parallelepiped, and \bar{n}_ξ , \bar{n}_η , and \bar{n}_ζ are the unit vectors along the parallelepiped primary edges in ξ , η , and ζ directions, respectively. Equation 19 defines a mapping between the deformation object (parallelepiped) and the grid point. The

grid points, \bar{r} , are mapped to the coordinates of the parallelepiped, ξ , η , and ζ , as

$$\begin{aligned} \xi &= \frac{\bar{n}_\eta \times \bar{n}_\zeta \cdot (\bar{r} - \bar{P}_0)}{\bar{n}_\eta \times \bar{n}_\zeta \cdot (\bar{n}_\xi)} \\ \eta &= \frac{\bar{n}_\xi \times \bar{n}_\zeta \cdot (\bar{r} - \bar{P}_0)}{\bar{n}_\xi \times \bar{n}_\zeta \cdot (\bar{n}_\eta)} \\ \zeta &= \frac{\bar{n}_\xi \times \bar{n}_\eta \cdot (\bar{r} - \bar{P}_0)}{\bar{n}_\xi \times \bar{n}_\eta \cdot (\bar{n}_\zeta)} \end{aligned} \quad (20)$$

A grid point is inside the parallelepiped if $0 \leq \xi, \eta, \zeta \leq 1$.

The FFD technique based on the parallelepiped is very efficient and easy to implement. It is suitable for local and global deformation. The only drawback is that the use of the parallelepiped limits the topology of deformation. To alleviate this drawback, Sederberg and Parry proposed to use nonparallelepiped objects.¹⁴ They also noted that the inverse mapping would be nonlinear and require significant computations.

Another popular method to define FFD is to use trivariate parametric volumes. Sederberg and Parry used a Bezier volume.¹⁴ Coquillart at INRIA extended Bezier parallelepiped to nonparallelepiped cubic Bezier volume.¹⁸ This idea has been further generalized to NURBS volume by Lamousin and Waggenspack.¹⁹ The NURBS blocks are defined as

$$\bar{r}(\xi, \eta, \zeta) = \frac{\sum_{i=0}^I N_{i,p1}(\xi) \sum_{j=0}^J N_{j,p2}(\eta) \sum_{k=0}^K N_{k,p3}(\zeta) W_{i,j,k} \bar{P}_{i,j,k}}{\sum_{i=0}^I N_{i,p1}(\xi) \sum_{j=0}^J N_{j,p2}(\eta) \sum_{k=0}^K N_{k,p3}(\zeta) W_{i,j,k}} \quad (21)$$

where N is the B-spline basis function, and the $p1$ – $p3$ are the degrees of N . The $\bar{P}_{i,j,k}$ are the NURBS control points that are related to the design variables. Lamousin and Waggenspack¹⁹ used multiple blocks to model complex shapes. This technique has been used for design and optimization by Yeh and Vance²⁰ and also by Perry and Balling.²¹

The common solid elements used in FE analysis (Fig. 14) can be used as deformation objects. The mapping from the solid element coordinates is defined²² by

$$\bar{r}(\xi, \eta, \zeta) = \sum_i \bar{P}_i N_i(\xi, \eta, \zeta) \quad (22)$$

where N_i are the FE basis functions, and \bar{P}_i are the nodal coordinates of deformation objects, which are related to the design variables. The equations for the inverse mapping is nonlinear for all solid elements with the exception of tetrahedron solid elements. The solid

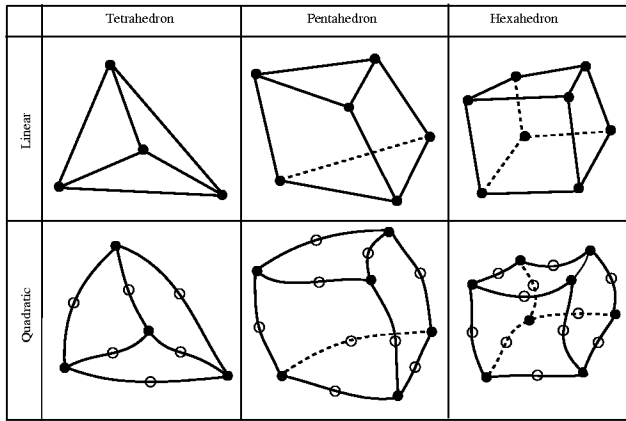


Fig. 14 FE solid elements.

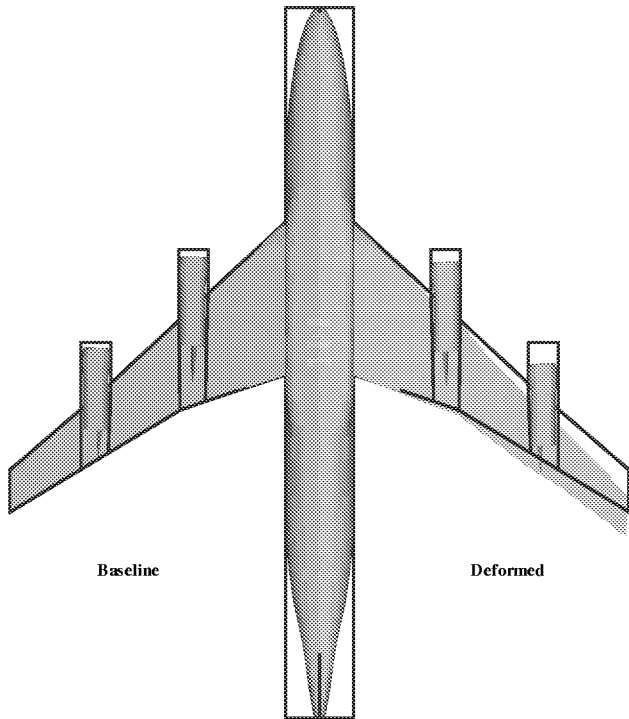


Fig. 15 Planform deformation of a transport.

elements provide a flexible environment to deform any shape. Complex shapes may require the use of several solid elements to cover the entire domain.

To model the planform shape, we have used hexahedron solid elements with four opposing edges parallel to the z -coordinate. Then, the planform design variables are linked to the corners of the hexahedral elements. Figure 15 shows the initial and deformed model for a transport configuration. The solid lines represent the controlling hexahedron solid elements. The baseline model is on the left-hand side; and the deformed shape is on the right-hand side.

As with the camber and thickness algorithms, the sensitivity of grid point coordinates is independent of the design variables ($\bar{P}_{id,jd}$) and coordinates (x, y, z). Thus, we need to calculate it only once, at the beginning of the optimization.

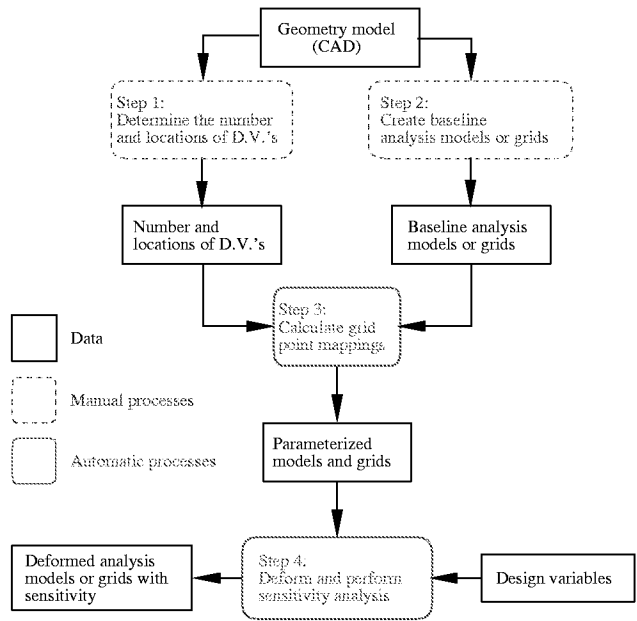


Fig. 16 Implementation plan.

Implementation

Figure 16 shows the implementation diagram for the combined algorithm. The implementation starts with a CAD model that defines the geometry. The first two steps can be implemented in parallel. The first step is to determine the number and the locations of the design variables with the aid of the CAD model. In the second step, the grids are manually generated for all involved disciplines. In the third step, the mappings described in the previous sections are calculated for each grid point. In the fourth step, the new grid is deformed in response to the new design variables, and the sensitivity derivatives are computed as well. The third and fourth steps are completely automated. The first three steps are considered preprocessing steps and need to be done only once.

Parameterizing Computational Structural Mechanics Models

Parameterizing CFD and CSM models appear to be similar in nature, but the CSM model parameterization has two additional requirements. First, the CSM model parameterization must include not only the OML but also the internal structural elements such as spars and ribs. Second, the deformed CSM model must be a valid design. For example, the spars must stay straight during the optimization. The algorithms presented in this paper can easily handle the first requirement. However, if the planform design variables are not selected with care, the second requirement could be easily violated. To avoid creating invalid CSM models, planform must be parameterized with few hexahedron solid elements, and they must be aligned with major structural components such as spar and ribs.

Results and Conclusions

The algorithms presented in this paper have been applied for parameterizing a simple wing, a blended wing body, and several high-speed civil transport configurations. Figure 17 shows the baseline and deformed grids for a high-speed civil transport. The solid lines represent the hexahedron solid elements controlling the planform variation. The parameterization results from this research have been successfully implemented for aerodynamic shape optimization with analytical sensitivity with structured⁷ and unstructured CFD grids.⁹ The parameterization algorithm presented in this paper is easy to implement for an MDO application with complex configuration. The resulting parameterization is consistent across all disciplines. Because the formulation is based on the SOA algorithms, the analytical sensitivity is also available. The algorithms are based on parameterizing the shape perturbations, thus enabling the parameterization of complex existing analysis models (grids). Another benefit of parameterizing the shape perturbation is that the process requires few design variables. Use of NURBS representation provides strong local control, and the smoothness can easily be controlled.

Acknowledgments

The author would like to thank James Townsend and Tom Zang of Multidisciplinary Optimization Branch of NASA Langley Research Center for reviewing this paper.

References

- ¹Samareh, J. A., "Status and Future of Geometry Modeling and Grid Generation for Design and Optimization," *Journal of Aircraft*, Vol. 36, No. 1, 1999, pp. 97–104.
- ²Samareh, J. A., "A Survey of Shape Parameterization Techniques," *AIAA/CEAS/ICASE/NASA-LaRC International Forum on Aeroelasticity and Structural Dynamics Conference*, Jun. 1999, accepted for publication.
- ³Haftka, R. T. and Grandhi, R. V., "Structural Shape Optimization—A Survey," *Computer Methods in Applied Mechanics and Engineering*, Vol. 57, 1986, pp. 91–106.
- ⁴Ding, Y., "Shape Optimization of Structures: A Literature Survey," *Computers & Structures*, Vol. 24, No. 6, 1986, pp. 985–1004.
- ⁵Watt, A. and Watt, M., *Advanced Animation and Rendering Techniques*, Addison-Wesley Publishing Company, New York, 1992.
- ⁶Samareh, J. A., "Computational Aerosciences in the 21st Century," ICASE, 1998, Presented at the ICASE/LaRC/NSF/ARO Workshop on Computational Aerosciences in the 21st Century, Hampton, Virginia, April 22–24, 1998.
- ⁷Biedron, R. T., Samareh, J. A., and Green, L. L., "Parallel Computation of Sensitivity Derivatives With Application to Aerodynamic Optimization of a Wing," *1998 Computer Aerosciences Workshop*, NASA CP–20857, Jan. 1999, pp. 219–224.
- ⁸Green, L. L., Weston, R. P., Salas, A. O., Samareh, J. A., and Townsend, J. C., "Engineering Overview of a Multidisciplinary HSCT Design Framework Using Medium-Fidelity Analysis Codes," *1998 Computer Aerosciences Workshop*, Jan. 1999, pp. 133–134.

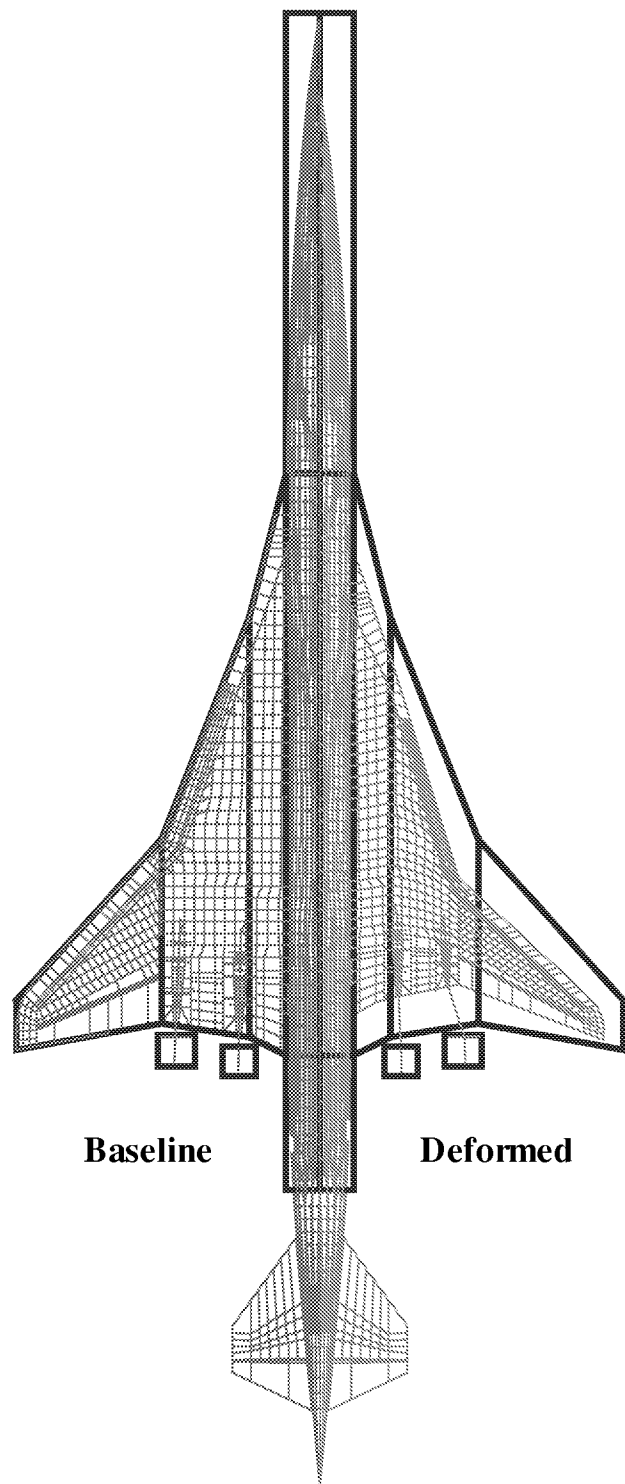


Fig. 17 Parameterization of the CSM Model of HSCT

⁹Nielsen, E. J. and Anderson, W. K., "Aerodynamic Design Optimization on Unstructured Meshes Using the Navier-Stokes Equations," *7th AIAA/USAF/NASA/ISSMO Symposium on Multidisciplinary Analysis and Optimization Conference Proceedings*, Sep. 1998, pp. 825–837, also AIAA-98-4809-CP.

¹⁰Hicks, R. M. and Henne, P. A., "Wing Design by Numerical Optimization," *Journal of Aircraft*, Vol. 15, No. 7, 1978, pp. 407–412.

¹¹Cosentino, G. B. and Holst, T. L., "Numerical Optimization Design of Advanced Transonic Wing Configurations," *Journal of Aircraft*, Vol. 23, No. 3, 1986, pp. 193–199.

¹²Hall, V., "Morphing in 2-D and 3-D," *Dr. Dobb's Journal*, Vol. 18, No. 7, 1993, pp. 18–26.

¹³Barr, A. H., "Global and Local Deformation of Solid Primitives," *Computer Graphics*, Vol. 18, No. 3, 1984, pp. 21–30.

¹⁴Sederberg, T. W. and Parry, S. R., "Free-Form Deformation of Solid Geometric Models," *Computer Graphics*, Vol. 20, No. 4, 1986, pp. 151–160.

¹⁵Abbott, I. A. and Von Doenhoff, A. E., *Theory of Wing Sections*, Dover Publications, New York, 1959.

¹⁶Farin, G., *Curves and Surfaces for Computer Aided Geometric Design*, Academic Press, New York, 1990.

¹⁷Sederberg, T. W. and Greenwood, E., "A Physically Based Approach to 2-D Shape Blending," *Computer Graphics*, Vol. 26, No. 2, 1992, pp. 25–34.

¹⁸Coquillart, S., "Extended Free-Form Deformation: A Sculpturing Tool for 3D Geometric Modeling," *SIGGRAPH*, Vol. 24, No. 4, 1990, pp. 187–196.

¹⁹Lamousin, H. J. and Waggenspack, W. N., "NURBS-Based Free-Form Deformation," *IEEE Computer Graphics and Applications*, Vol. 14, No. 6, 1994, pp. 95–108.

²⁰Yeh, T.-P. and Vance, J. M., "Applying Virtual Reality Techniques to Sensitivity-Based Structural Shape Design," *Proceedings of 1997 ASME Design Engineering Technical Conferences*, No. DAC-3765 in DETC97, Sep. 1997, pp. 1–9.

²¹Perry, E. and Balling, R., "A New Morphing Method for Shape Optimization," Paper 98-2896, AIAA, Jun. 1998.

²²Cook, R. D., Malkus, D. S., and Plesha, M. E., *Concepts and Applications of Finite Element Analysis*, John Wiley & Sons, New York, 1989.

REPORT DOCUMENTATION PAGE

Form Approved
OMB No. 0704-0188

Public reporting burden for this collection of information is estimated to average 1 hour per response, including the time for reviewing instructions, searching existing data sources, gathering and maintaining the data needed, and completing and reviewing the collection of information. Send comments regarding this burden estimate or any other aspect of this collection of information, including suggestions for reducing this burden, to Washington Headquarters Services, Directorate for Information Operations and Reports, 1215 Jefferson Davis Highway, Suite 1204, Arlington, VA 22202-4302, and to the Office of Management and Budget, Paperwork Reduction Project (0704-0188), Washington, DC 20503.

| | | | | |
|---|---|--|--|--|
| 1. AGENCY USE ONLY (Leave blank) | | 2. REPORT DATE May 1999 | 3. REPORT TYPE AND DATES COVERED Technical Memorandum | |
| 4. TITLE AND SUBTITLE A Novel Shape Parameterization Approach | | | 5. FUNDING NUMBERS WU 509-10-11-01 | |
| 6. AUTHOR(S) Jamshid A. Samareh | | | | |
| 7. PERFORMING ORGANIZATION NAME(S) AND ADDRESS(ES) NASA Langley Research Center Hampton, VA 23681-2199 | | | 8. PERFORMING ORGANIZATION REPORT NUMBER L-17841 | |
| 9. SPONSORING/MONITORING AGENCY NAME(S) AND ADDRESS(ES) National Aeronautics and Space Administration Washington, DC 20546-0001 | | | 10. SPONSORING/MONITORING AGENCY REPORT NUMBER NASA/TM-1999-209116 | |
| 11. SUPPLEMENTARY NOTES | | | | |
| 12a. DISTRIBUTION/AVAILABILITY STATEMENT Unclassified-Unlimited Subject Category 64 Distribution: Standard Availability: NASA CASI (301) 621-0390 | | | 12b. DISTRIBUTION CODE | |
| 13. ABSTRACT (Maximum 200 words) This paper presents a novel parameterization approach for complex shapes suitable for a multidisciplinary design optimization application. The approach consists of two basic concepts: (1) parameterizing the shape perturbations rather than the geometry itself and (2) performing the shape deformation by means of the soft objects animation algorithms used in computer graphics. Because the formulation presented in this paper is independent of grid topology, we can treat computational fluid dynamics and finite element grids in a similar manner. The proposed approach is simple, compact, and efficient. Also, the analytical sensitivity derivatives are easily computed for use in a gradient-based optimization. This algorithm is suitable for low-fidelity (e.g., linear aerodynamics and equivalent laminated plate structures) and high-fidelity analysis tools (e.g., nonlinear computational fluid dynamics and detailed finite element modeling). This paper contains the implementation details of parameterizing for planform, twist, dihedral, thickness, and camber. The results are presented for a multidisciplinary design optimization application consisting of nonlinear computational fluid dynamics, detailed computational structural mechanics, performance, and a simple propulsion module. | | | | |
| 14. SUBJECT TERMS Shape, Optimization, Parameterization, CFD, CSM, Geometry, Grid Generation, Soft Object Animation, Free-Form Deformation, Sensitivity Analysis, Multidisciplinary Design Optimization, MDO, Airplane Design | | | 15. NUMBER OF PAGES 15 | |
| | | | 16. PRICE CODE A03 | |
| 17. SECURITY CLASSIFICATION OF REPORT Unclassified | 18. SECURITY CLASSIFICATION OF THIS PAGE Unclassified | 19. SECURITY CLASSIFICATION OF ABSTRACT Unclassified | 20. LIMITATION OF ABSTRACT | |